Accuracy of Simplifications for Spectral Responsivity Measurements of Solar Cells

Karsten Bothe, David Hinken, Byungsul Min, and Carsten Schinke

***Abstract*—The determination of the spectral responsivity is an essential part of solar cell characterization. Since solar simulators only approximate the reference spectrum, a spectral mismatch correction has to be performed. This correction procedure requires spectral responsivity data. Apart from the complete differential spectral responsivity procedure, the IEC 60904-8 standard defines four simplifications. In this paper, we provide information on the variations in the spectral responsivity curves for these simplifications. We show that for nonlinear front junction cells, deviations predominantly occur at wavelengths above 700 nm and become largest around 1000 nm. While we found a maximum deviation of 30% for the simplification with lowest requirements in bias irradiance, all other simplifications yield deviations below 10%. For a nonlinear cell measured relative to a world photovoltaic scale reference cell using a class A solar simulator, this transfers to a deviation below 0.01% in the spectral mismatch factor. If one depends on the use of a simplification, we recommend using the multicolor approach. Even though the singlecolor approach might yield lower deviations, this approach requires knowledge about the maximum in the spectral responsivity, which is not generally known in advance of the measurement. Accepting a slightly higher deviation, the white bias approach is a recommendable alternative.**

***Index Terms*—Calibration, IEC 60904-8, solar cell, spectral mismatch, spectral responsivity.**

I. Introduction

THE determination of the characteristic solar cell parameters in accordance to the IEC 60904 standards requires the use of the AM1.5 global spectral distribution (defined in the IEC 60904-3 standard). However, solar simulators can only approximate the required spectral distribution. Thus, a spectral mismatch correction (accounting for deviations between the solar simulator and the solar reference spectral distribution as well as for differences in the spectral responsivity of the reference cell and the cell under test) has to be performed in order to obtain accurate values of the short-circuit current under standard test conditions $I_{\mathrm{SC.STC}}$. In order to calculate the required spectral mismatch factor (MM), the spectral responsivity of the test cell has to be measured. The requirements for the measurement of the spectral responsivity of linear and nonlinear photovoltaic devices are defined in the IEC 60904-8 standard.

In May 2014, Edition 3 of the IEC 60904-8 [1] standard was published. For highest accuracy, the standard demands to measure the complete differential spectral responsivity procedure. This approach requires differential spectral responsivity curves $\tilde{s}(\lambda, I_{\mathrm{bias}}(E_{\mathrm{bias}}))$ of a cell as a function of wavelength λ under at least five different bias light irradiances E_{bias}. The bias light irradiances are adjusted to yield bias currents I_{bias} between 5% and 110% of the short-circuit current. Apart from this complete differential spectral responsivity procedure, the standard names four simplified procedures. These simplifications determine an appropriate bias current $I_{\mathrm{bias}}(E_0)$ at which the measured differential spectral responsivity equals the calculated spectral responsivity of the solar cell under test.

This paper aims at providing information on the accuracy of the proposed simplifications. Therefore, the complete differential spectral responsivity procedure and all four simplifications are determined for nonlinear solar cells by means of device simulations and experiments. The resulting curves are compared with each other and the deviation of the simplifications to the complete differential spectral responsivity procedure is calculated. In addition, we comment on the corresponding deviations in the spectral mismatch factor.

II. Spectral Responsivity in Solar Cell Calibration

The responsivity

$$s = \frac{I_{\mathrm{SC}}}{E} \tag{1}$$

specifies the short-circuit current I_{SC} of a cell generated per unit irradiance E.

As the responsivity of a solar cell is wavelength-dependent, its value critically depends on the spectral distribution of the light source used for the performance measurement. Consequently, performance measurements carried out under natural sunlight can vary by as much as 15% from day-to-day at the same place, if only the irradiance is measured with a spectrally nonselective thermopile-type radiometer [2] instead of measuring the spectral distribution. Under state-of-the-art solar simulators day-to-day variations are considerably smaller.

Aiming at intercomparability of measurements at different laboratories, the characteristic solar cell parameters have to be determined at standard testing conditions (STC) [3].

In primary solar cell calibration [4], the spectral responsivity related to STC $s_{\mathrm{STC}}(\lambda)$ is used to determine the related

Manuscript received August 10, 2017; revised November 9, 2017 and January 5, 2018; accepted January 9, 2018. Date of publication February 7, 2018; date of current version February 16, 2018. (*Corresponding author: Karsten Bothe.*)

K. Bothe, D. Hinken, and B. Min are with the Institut für Solarenergieforschung, Emmerthal 31860, Germany (e-mail: k.bothe@isfh.de; d.hinken@isfh.de; b.min@isfh.de).

C. Schinke is with the Institute for Solid State Physics, Leibniz Universität Hannover, Hannover 30167, Germany (e-mail: schinke@solar.uni-hannover.de).

Color versions of one or more of the figures in this paper are available online at http://ieeexplore.ieee.org.

Digital Object Identifier 10.1109/JPHOTOV.2018.2793758

short-circuit current according to the following equation:

$$I_{\mathrm{SC.STC}} = \int_0^\infty s_{\mathrm{STC}}(\lambda) E_{\mathrm{AM15}}(\lambda)\, d\lambda. \tag{2}$$

The spectral responsivity

$$s(\lambda) = \frac{I_{\mathrm{SC}}(\lambda)}{E(\lambda)} \tag{3}$$

in units of $\mathrm{AW}^{-1}\mathrm{m}^2$ is determined by irradiating the device by means of a narrow-bandwidth light at a series of different wavelengths λ covering its responsivity range, and measuring the monochromatic short-circuit current $I_{\mathrm{sc}}(\lambda)$ as well as the monochromatic irradiance $E(\lambda)$ at each of these wavelengths.

The spectral responsivity at standard test conditions $s_{\mathrm{STC}}(\lambda)$ will equal the spectral responsivity $s(\lambda)$ only if the device is strictly linear. For nonlinear solar cells $I_{\mathrm{SC}}(\lambda)$ is a function of the bias current $I_{\mathrm{bias}}(E_{\mathrm{bias}})$, which is generated by a bias irradiance E_{bias} and the spectral responsivity has to be calculated from the differential spectral responsivity

$$\tilde{s}\,(\lambda, I_{\mathrm{bias}}) = \left.\frac{\partial I_{\mathrm{SC}}\,(\lambda, E)}{\partial E}\right|_{I_{\mathrm{bias}}}. \tag{4}$$

A nonlinearity may result from an injection-dependent carrier recombination predominantly occurring in the bulk or at a dielectric rear of a solar cell [5], [6].

The integration over I_{bias} up to $I_{\mathrm{SC.STC}}$ yields the (nondifferential) spectral responsivity related to standard test conditions

$$s_{\mathrm{STC}}(\lambda) = \frac{I_{\mathrm{SC.STC}}}{\int_0^{I_{\mathrm{SC.STC}}} \frac{1}{\tilde{s}(\lambda, I_{\mathrm{bias}})} dI_{\mathrm{bias}}}\ . \tag{5}$$

The required $I_{\mathrm{SC.STC}}$ is determined in two steps. In the first step, the AM1.5G-weighted differential responsivities

$$\tilde{s}_{\mathrm{AM1.5}}\,(I_{\mathrm{bias}}) = \frac{\int_0^\infty \tilde{s}\,(\lambda, I_{\mathrm{bias}})\, E_{\mathrm{AM1.5}}(\lambda) d\lambda}{\int_0^\infty E_{\mathrm{AM1.5}}(\lambda) d\lambda} \tag{6}$$

are calculated, which yield the responsivity under STC conditions

$$s\,(I_{\mathrm{SC.STC}}) = \frac{I_{\mathrm{SC.STC}}}{\int_0^{I_{\mathrm{SC.STC}}} \frac{1}{\tilde{s}_{\mathrm{AM15}}(I_{\mathrm{bias}})} dI_{\mathrm{bias}}}. \tag{7}$$

In the second step, $I_{\mathrm{SC.STC}}$ is determined by iteratively increasing the upper limit of the integral in the denominator of (7) until the denominator equals 1000 $\mathrm{W{\cdot}m^{-2}}$.

In secondary solar cell calibration, the spectral responsivity is required for the spectral mismatch correction procedure that accounts for deviations between the solar simulator spectrum and the solar reference spectral irradiance as well as for differences in the spectral responsivity of the reference cell (ref) and the cell under test. In contrast with primary solar cell calibration aiming at directly determining $I_{\mathrm{SC.STC}}$ from the spectral responsivity, the calculation of the spectral mismatch factor

$$\mathrm{MM} = \frac{\int E_{\mathrm{AM15}}(\lambda) s_{\mathrm{STC.rel.ref}}(\lambda) d\lambda \int E_{\mathrm{meas}}(\lambda) s_{\mathrm{STC.rel}}(\lambda) d\lambda}{\int E_{\mathrm{meas}}(\lambda) s_{\mathrm{STC.rel.ref}}(\lambda) d\lambda \int E_{\mathrm{AM15}}(\lambda) s_{\mathrm{STC.rel}}(\lambda) d\lambda} \tag{8}$$

according to the IEC 60904-7 [7] standard only requires the *relative* spectral responsivity curve $s_{\mathrm{rel}}(\lambda)$, which may differ from the spectral responsivity by a wavelength-independent scaling factor. The quantities $E_{\mathrm{meas}}(\lambda)$ and $E_{\mathrm{AM15}}(\lambda)$ are the sun simulator and tabulated reference spectrum, respectively.

III. Determination of Spectral Responsivity Curves

In order to account for nonlinear solar cells when determining the MM from the spectral responsivity, the IEC 60904-8 standard defines in Section 7.5 a procedure for highest accuracy as well as four simplifications. These simplifications might increase the measurement uncertainty but have the advantage of shorter measurement times and allow the use of less complex and cheaper equipment.

A. Complete Differential Spectral Responsivity Procedure

The reference approach, for the determination of the spectral responsivity $s_{\mathrm{STC}}(\lambda)$ (as introduced in principle in the previous section) requires the measurement of $\tilde{s}(\lambda, I_{\mathrm{bias}})$ under at least five different bias light irradiances, which result in short-circuit currents I_{bias} ranging from 5% to 110% of the short-circuit current of the solar cell under standard test conditions.

B. Simplifications

1) Multicolor and Singlecolor Approach: If the complete differential spectral responsivity procedure cannot be performed, a bias light irradiance E_0 has to be determined at which the differential spectral responsivity best approximates the spectral responsivity of the device under test. For the multicolor approach, the differential spectral responsivity $\tilde{s}(\lambda_i, I_{\mathrm{bias}})$ has to be measured with a step width of 200 nm (i.e., for crystalline silicon at three to five different wavelengths λ_i) or, for the singlecolor approach, at least at one wavelength λ_1 close to the maximal spectral responsivity at three to five different bias light irradiances E_{bias}. The bias light irradiances shall result in bias currents I_{bias} ranging from approximately 5% to approximately 110% of the approximated[1] short-circuit current $I_{\mathrm{SC.STC.approx}}$ of the device under test. The set of differential spectral responsivities as a function of bias irradiance is named bias ramp. For each bias ramp the spectral responsivity is calculated using (5) from the differential spectral responsivity and the bias current $I_{\mathrm{bias}}(E_{0\mathrm{i}})$ at which the measured differential responsivity equals the calculated spectral responsivity is determined. Finally, the differential spectral responsivity over the whole wavelength range is measured, while the used bias light is adapted to $I_{\mathrm{bias}}(E_{0\mathrm{i}})$ and its corresponding wavelength region.

2) White Bias Approach: If the first simplification cannot be performed, the bias light irradiance E_0 shall be determined by using white light instead of monochromatic light. At three to five different bias light irradiances E_{bias}, the differential white light responsivity $\tilde{s}_{\mathrm{WL}}(I_{\mathrm{bias}})$ has to be measured. Again, the bias light irradiances shall result in bias currents I_{bias} ranging from

[1]The term "approximated" short-circuit current is used, since the spectral distribution of the bias light might differ from the reference spectrum and no spectral mismatch correction is applied.

approximately 5% to approximately 110% of the approximated short-circuit current of the device under test.

3) One-Third Approach: If the measurement setup does not allow to use one of the methods described above, a bias light level that generates a short-circuit current of 30% to 40% of $I_{\mathrm{SC.STC.approx}}$ shall be used. The measured differential spectral responsivity is assumed to equal the spectral responsivity at standard test conditions.

4) Low Bias Approach: If all this cannot be realized, a bias light level that generates a short-circuit current of at least 10% $I_{\mathrm{STC.approx}}$ can be used. It has to be verified that the monochromatically generated current in the device under test as function of wavelength does not vary by more than 2% if the bias light irradiance is 1) reduced to 50% and 2) increased by 50%. If it varies by more than 2%, the two additional measurement curves have to be included in the measurement report.

Within this paper, we analyze the proposed simplifications. By means of device simulations and experimental measurements, we compare the $s_{\mathrm{STC}}(\lambda)$ -curves determined according to the different simplifications with the result following from the complete differential spectral responsivity procedure.

IV. Simulation Details

A. Simulation Software

The basis of the simulation forms the general purpose device simulation tool SENTAURUS [8]. A frontend developed at Institut für Solarenergieforschung simplifies the generation of the required input files, runs the simulation, and carries out a postprocessing of the data when the simulation has finished. As a first step, optical simulations [9] are performed with the ray-tracing module of SENTAURUS to provide all carrier generation profiles required for the electrical device simulation. The optical simulation uses a three-dimensional symmetry element consisting of one-quarter of an upright pyramid of the front surface texture and the corresponding base and rear part of the solar cell. For each monochromatic wavelength and for the bias irradiance, separate generation profiles are generated, which can later be fed into the electrical device simulation.

B. Simulation Procedure

To simulate the differential spectral responsivity curves, two device simulations where the solar cell is held at zero voltage and the extracted current is determined are required. First, a simulation with bias irradiance I_{bias} only, giving the short-circuit current $I_{\mathrm{sc.1}}$. Second, a simulation with bias irradiance I_{bias} superimposed by the monochromatic light with wavelength λ and irradiance intensity E_λ, giving the short-circuit current $I_{\mathrm{sc.2}}$. The differential spectral responsivity is then calculated by the following equation:

$$\tilde{s}\,(\lambda, I_{\mathrm{bias}}) = \frac{I_{\mathrm{sc.2}} - I_{\mathrm{sc.1}}}{E_\lambda}\,. \tag{9}$$

C. Simulated Solar Cell

For the simulated solar cell, most recent silicon parameters and device models are applied from [9]–[14]. The cell has a 180 μm thick boron-doped Cz–Si base. The Shockley-Read-Hall (SRH) lifetime is modeled with the parametrization given in [15] by assuming that the limiting SRH defect is the B–O complex having $\tau_p/\tau_n = 10$, concretely $\tau_n = 80\,\mu$s and $\tau_p = 800\,\mu$s. We apply the results of electrochemical capacitance–voltage measurements of published experiments [16], [17] as dopants profiles for the *n*-type emitter on the front surface resulting in a saturation current density of $J_{0\mathrm{e}} = 59\,\mathrm{fA/cm^2}$. The cell is textured with upright pyramids and feature an SiN_x antireflective coating with a thickness of 78 nm. The rear side is optically approximated with a planar geometry with a scattering described with Phong's model [18]. The passivation of the rear side is achieved with a silicon dioxide dielectric layer. The recombination at the interface is modeled with the parameters given in [6] and [19] by assuming energy-independent capture cross sections of electrons and holes. A positive fixed oxide charge of 5×10^{10} cm^{-2} (silicon oxide) is assumed.

The simulated solar cell is of size 1 cm² and features a short-circuit current $I_{\mathrm{SC.STC}}$ of 40.57 mA, an open-circuit voltage V_{oc} of 655.6 mV, a fill factor (FF) of 80.24% and an efficiency η of 21.34%.

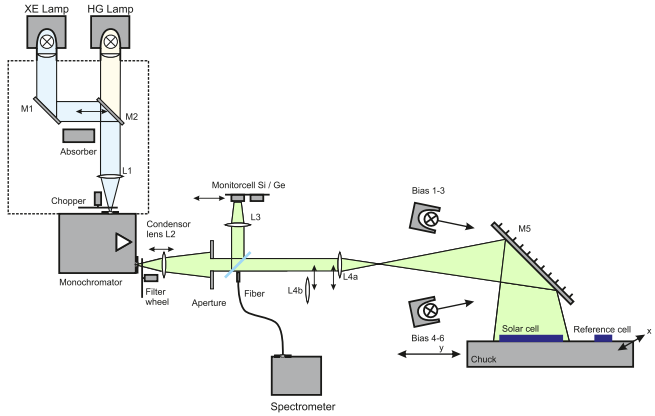

Fig. 1. Schematic representation of the differential spectral responsivity measurement setup at ISFH CalTeC. All mirrors are named M while all lenses are named L. The chuck is mounted on a x-y stage allowing to irradiate either the reference or the solar cell under test.

V. Experimental Details

A. Measurement Apparatus

A schematic representation of the spectral responsivity measurement apparatus used in this study is shown in Fig. 1. It consists of two light sources, a chopper wheel, a grating monochromator, a beam splitting assembly for beam irradiance monitoring, two monitor detectors, a large rear mirror, a moveable stage that holds the device under test and the reference device, a bias light assembly, three transimpedance amplifiers, and a two-channel lock-in amplifier. The measurement apparatus realizes a dual beam arrangement consisting of a bias light beam constant in time superimposed by a pulsed monochromatic beam. The wavelength of the monochromatic light can be adjusted between 280 and 1200 nm and has a bandwidth of about 10 nm. Using the beam splitting assembly, the monochromatic light beam is split into a low intensity monitor beam and a high intensity measurement beam. The monitor beam is

measured using a silicon diode for the wavelengths below 660 nm and a germanium diode for the wavelengths above. The monitor signal is used to correct for fluctuations in the monochromatic light intensity. A secondary reflection of the monitor beam is detected with an array spectrometer and serves for monitoring the wavelength and bandwidth of the monochromatic light. The measurement beam is expanded and homogenized by a set of optical lenses to an area of either 160 × 160 mm^2 or 50 × 50 mm^2, respectively. Bias light is generated by an array of up to 48 dichroic halogen lamps.

The system features two different measurement chucks. The first is specially designed to mount world photovoltaic scale (WPVS) reference solar cells [20]. The second allows to mount solar cells sizing from 10 × 10 mm² up to 160 × 160 mm². The temperature stabilization of the solar cells on both chucks is realized with water-cooled peltier elements. Temperature ranges from 20 °C to 50 °C are feasible with an excellent stabilization of ±20 mK.

Either the reference cell or the solar cell under test is irradiated simultaneously with the chopped monochromatic light of low intensity and the bias light of considerably higher intensity. The response of the solar cell to this irradiation is a short-circuit current consisting of a constant and a pulsed part. The transimpedance amplifier separates the pulsed part of the short-circuit current and transforms it into a proportional voltage, which is measured by a lock-in amplifier.

B. Measurement Procedure

Before measuring the solar cell under test, the monochromatic irradiances of the measurement apparatus have to be calibrated. For this, the bias current of the primary calibration is reproduced and the signal of the reference cell i_{ref} as well as that of the internal monitor diode $i_{\mathrm{ref.mon}}$ is recorded. This procedure yields the transfer function

$$k(\lambda) = \tilde{s}_{\mathrm{ref}}(\lambda) \cdot \frac{i_{\mathrm{ref.mon}}(\lambda)}{i_{\mathrm{ref}}(\lambda)} \tag{10}$$

where $\tilde{s}_{\mathrm{ref}}(\lambda)$ is the differential spectral responsivity as given in the calibration certificate of the reference cell. After calibration the test cell is mounted and contacted. The differential spectral responsivity $\tilde{s}(\lambda, I_{\mathrm{bias}})$ of the solar cell under test at a bias current I_{bias} follows according to the following equation:

$$\tilde{s}\,(\lambda, I_{\mathrm{bias}}) = \; k(\lambda) \cdot \frac{i_{\mathrm{test}}\,(\lambda, I_{\mathrm{bias}})}{i_{\mathrm{test.mon}}(\lambda)} \tag{11}$$

where i_{test} and $i_{\mathrm{test.mon}}$ are the measured signals of the solar cell under test and the monitor diode, respectively.

In case the active area of the reference solar cell and of the solar cell under test differs, a homogeneity correction factor, determined by scanning the light field for each wavelength, corrects for remaining lateral inhomogeneities of the light field.

For the measurement of the complete differential spectral responsivity procedure, we measure the differential spectral responsivity for the complete spectral range at bias irradiances of approximately 10, 25, 100, 200, 300, 1000, and 1100 W/m^2. For the measurement of the monochromatic bias ramps, irradiances of approximately 10, 25, 100, 200, 300, 400, 600, 800, 1000, and 1100 W/m² are used.

The white bias ramp is determined in the same way as the monochromatic bias ramp except that chopped white light is used instead of monochromatic light. Technically, the white light is obtained by using the zero order position of one of the gratings in combination with the halogen lamp. By reducing the width of the monochromator exit slit, the intensity of the chopped white light is adjusted to an appropriate smaller value.

C. Measured Solar Cell

For the measurements, we investigated different types of solar cells to select one with a very strong non-linearity, since only for such a cell the simplifications of the complete differential spectral responsivity procedure might yield divergent results. We found nonlinearities for solar cells

1) with a strongly injection-dependent charge carrier lifetime in the base caused by contamination with iron;
2) with a silicon dioxide/silicon nitride dielectric rear stack;
3) with only a silicon nitride rear layer.

Solar cell 3) showed the strongest nonlinearity and will thus be used as solar cell under test for the experimental analysis. This solar cell is a crystalline silicon wafer cell with a size of 156 × 156 mm^2. It is an industrial-type monocrystalline *p*-type Czochralski (Cz) silicon passivated emitter and rear- type solar cell. The standard version of this cell structure [21] has a rear side passivation stack consisting of an aluminum oxide (Al_2O_3) and a silicon nitride (Si_3N_4) layer. In contrast with this, the Al_2O_3 layer was omitted for this solar cell to obtain a rear surface recombination velocity with a high injection dependence.

The investigated solar cell features a short-circuit current $I_{\mathrm{SC.STC}}$ of 9151 mA, an open-circuit voltage V_{oc} of 645.7 mV, an FF of 71.60%, and an efficiency η of 17.27%. Note that the FF is so small because of the strong injection dependence of that cell.

VI. Resulting Spectral Responsivity Curves

A. Complete Differential Spectral Responsivity Procedure

Figs. 2 and 3 show the simulated and measured differential spectral responsivity curves as a function of wavelength for bias currents I_{bias} between 1.9 and 48.9 mA (simulation) and 78 and 9971 mA (measurement), respectively. Apart from the differential spectral responsivity curves $\tilde{s}(\lambda, I_{\mathrm{bias}})$, Figs. 2 and 3 also show the calculated spectral responsivity $s_{\mathrm{STC}}(\lambda)$ in red.

As expected for solar cells featuring an injection-dependent rear surface or bulk recombination, the differential spectral responsivity is a function of the bias irradiance for wavelengths above 700 nm. From the direct comparison of Fig. 2 and Fig. 3, we see the bias dependence of the simulated data starting already at slightly shorter wavelengths, thus indicating a stronger injection dependence of the simulated cell.

B. Simplifications

1) Multicolor and Singlecolor Approach: In accordance to the multicolor approach, Figs. 4 (simulated data) and 5

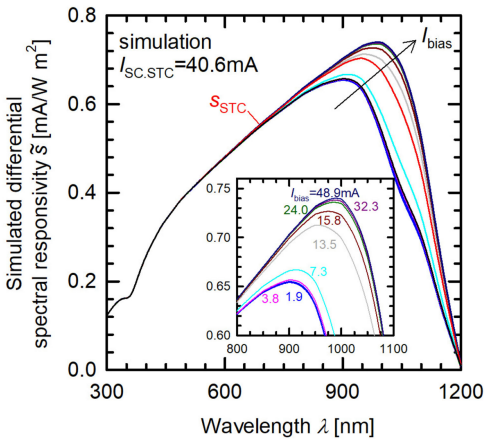

Fig. 2. Simulated differential spectral responsivity $\tilde{s}(\lambda,\ I_{\mathrm{bias}})$ of a nonlinear solar cell featuring a silicon oxide dielectric rear surface with an injection-dependent rear surface recombination velocity. In addition, the spectral responsivity related to standard test conditions $s_{\mathrm{STC}}(\lambda)$ is shown in red.

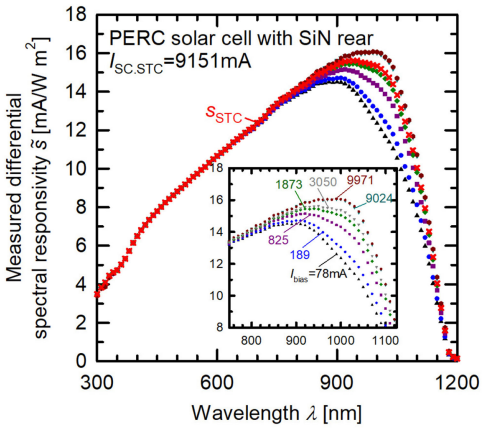

Fig. 3. Measured differential spectral responsivity of the chosen nonlinear crystalline silicon solar cell. The nonlinearity stems from an omitted Al_2O_3-layer at the rear. In addition, the spectral responsivity related to standard test conditions is shown in red.

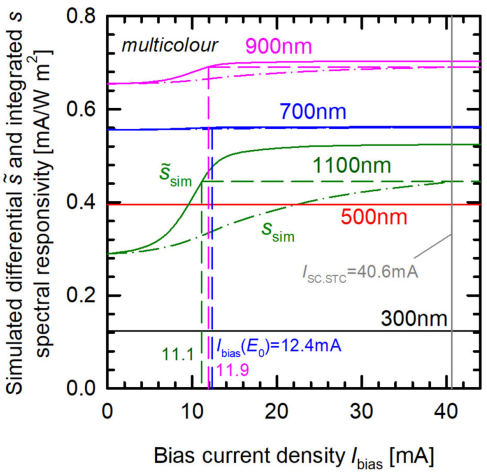

Fig. 4. Multicolor approach: Simulated monochromatic bias ramps for different wavelengths λ_i. Bias currents $I_{0i} = I_{\mathrm{bias}}(E_{0i})$, at which $\tilde{s}(\lambda_i, I_{0i})$ equals $s_{\mathrm{STC}}(\lambda_i)$, are provided for 700, 900 and 1100 nm.

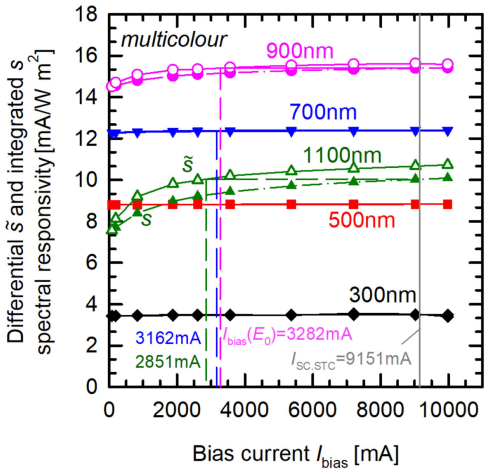

Fig. 5. Multicolor approach: Measured monochromatic bias ramps for different wavelengths λ_i. Bias currents $I_{0i} = I_{\mathrm{bias}}(E_{0i})$, at which $\tilde{s}(\lambda_i, I_{0i})$ equals $s_{\mathrm{STC}}(\lambda_i)$, are provided for 700, 900, and 1100 nm.

(measured data) show five simulated bias ramps $\tilde{s}(\lambda_i, I_{\mathrm{bias}})$ (solid lines) equally spaced in wavelength (at 300, 500, 700, 900, and 1100 nm). In addition to the differential spectral responsivity bias ramps, Figs. 4 and 5 also show the integrated spectral responsivity bias ramps $s(\lambda_i, I_{\mathrm{bias}})$ (dashed–dotted lines) for the same wavelength.

As expected, for a nonlinear cell with an injection-dependent rear surface recombination, the differential and integrated responsivity bias curves do not deviate for short-wavelength light (300 and 500 nm). The deviation is very small for 700 nm and becomes increasingly stronger for longer wavelengths (900 above 1100 nm). For the wavelengths 700, 900, and 1100 nm, the bias currents $I_{0i} = I_{\mathrm{bias}}(E_{0i})$, where $\tilde{s}(\lambda_i, I_{0i})$ equals $s_{\mathrm{STC}}(\lambda_i)(= s(\lambda_i, I_{\mathrm{sc.STC}}))$ are indicated. For the shorter wavelength, the spectral responsivity does not depend on the bias irradiance and thus any irradiance can be used. We use the same bias irradiance as for 700 nm to reduce the number of changes in E_{0i} for a shorter measurement time. For the simulated data, the multicolor determines a bias current of 12.4 mA for wavelengths up to 800 nm, of 11.9 mA from 800 to 1000 nm, and 11.1 mA from 1000 to 1200 nm. For the measured data, multicolor approach determines a bias current of 3282 mA up to 800 nm, of 3162 mA from 800 to 1000 nm, and 2851 mA from 1000 to 1200 nm.

The singlecolor approach shall use a bias ramp with a wavelength close to the maximal spectral responsivity. The spectral responsivity curves shown in Figs. 2 (simulation) and 3 (measurement) have maxima values between 900 and 1000 nm, where the values closer to 1000 nm correspond to a better rear passivation quality. Thus, we choose a wavelength of 1000 nm for the singlecolor approach, which is also a common choice for silicon devices featuring a front junction. The resulting differential spectral responsivity curves and the calculated spectral responsivity for 1000 nm are shown as blue lines in Fig. 6 (simulation) and Fig. 7 (measurement), respectively. The singlecolor approach yields a bias current of 11.4 mA (simulation)

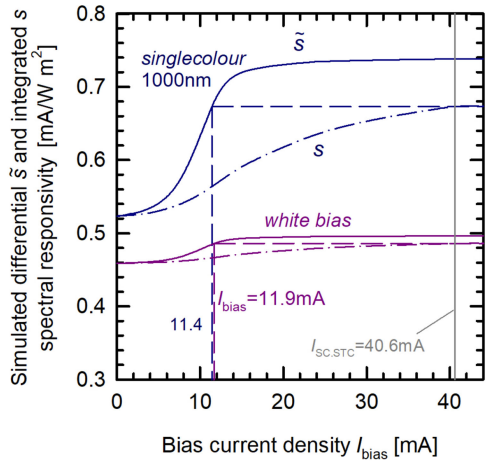

Fig. 6. Singlecolor approach (blue line) and white bias approach (purple line) of the simulated solar cell. Resulting $I_{\mathrm{bias}}(E_{0i})$ bias currents are denoted within the figure.

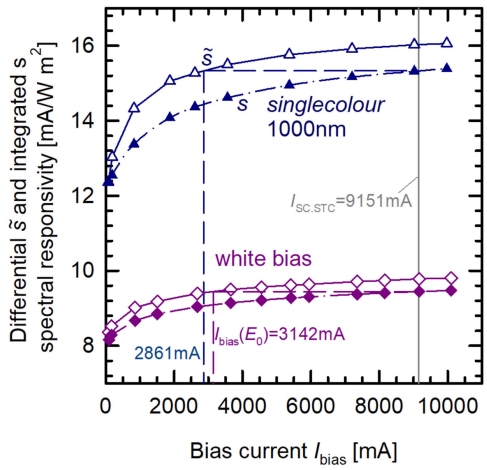

Fig. 7. Singlecolor approach (blue line) and white bias approach (purple line) of the measured data. Resulting $I_{\mathrm{bias}}(E_{0i})$ bias currents are denoted within the figure.

and 2861 mA (measurement), respectively. These values are between those determined from the bias ramps determined at 900 and 1100 nm, respectively.

2) White Bias Approach: The second simplification ("white bias approach") demands using white instead of monochromatic light to determine E_0 from a white light responsivity $\tilde{s}_{\mathrm{WL}}(I_{\mathrm{bias}}(E_{\mathrm{bias}}))$ curve. For the investigated cells, the result of this white bias approach is shown with purple lines in Fig. 6 (simulation) and Fig. 7 (measurement), respectively. The resulting $I_{\mathrm{bias}}(E_0)$ value is 11.7 mA (simulation) and 3142 mA (measurement), respectively. Compared with the $I_{\mathrm{bias}}(E_0)$ value determined from monochromatic bias ramps, the value from the white-bias approach corresponds to the highest bias irradiance.

3) One-Third Approach: For the one-third approach, a fixed bias current between 30% and 40% of $I_{\mathrm{SC.STC.approx}}$ is required. We use $I_0 = 1/3 \cdot I_{\mathrm{SC.STC}}$, which gives 13.5 mA (simulation) and 3050 mA (measurement). The resulting differential spectral responsivity curves are shown as gray curves in Fig. 2 (simulation) and Fig. 3 (measurement), respectively. Note that

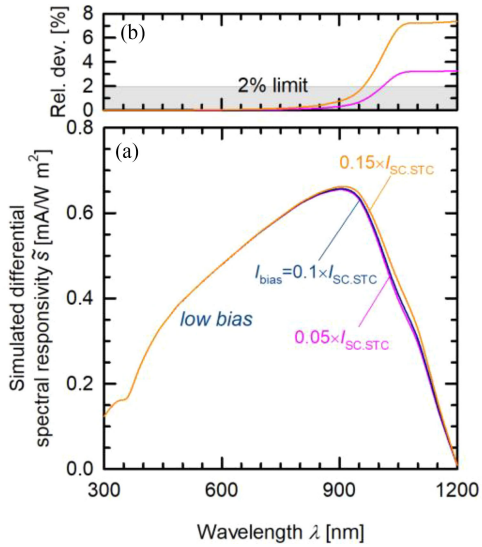

Fig. 8. Simulated data: (a) Spectral responsivity curves according to the low bias approach: 5%-, 10%- and 15%-curves. (b) Relative deviation of the 0.10- and 0.15-$I_{\mathrm{SC.STC}}$ curves to the 0.10-curve, exceeding the 2% limit at wavelengths larger than 950 nm (15%-curve) and 1000 nm (5%-curve).

the bias current of 13.5 mA as determined for the simulated cell is well above those values determined by the multicolor approach (12.4, 11.9 and 11.1 mA), the singlecolor approach (11.4 mA), and the white bias approach (11.7 mA). This is not the case for the measured data. The bias current of 3050 mA for the one-third approach is in-between the bias currents of the multicolor approach (3282, 3162, and 2851 mA), higher than the one of the singlecolor approach (2861 mA) and smaller than the white bias approach (3142 mA).

4) Low Bias Approach: The fourth simplification uses three fixed bias irradiances with low intensities. For the primary spectral responsivity curve, only 10% of $I_{\mathrm{SC.STC.approx}}$ as bias irradiance is needed. For the two secondary spectral responsivity curves, the bias irradiance has to be reduced to 50% and increased by 50% resulting in bias currents of 5% and 15% of $I_{\mathrm{SC.STC.approx}}$. The resulting curves are shown in Fig. 8(a) (simulation) and Fig. 9(a) (measurement), respectively. The corresponding relative deviation of the 5%- and the 15%-curve to the 10%-curve are shown in Fig. 8(b) (simulation) and in Fig. 9(a) (measurement), respectively. For both cells studied here, the differential spectral responsivity curves start to deviate at wavelengths above 800 nm. The deviation exceeds the 2% limit defined in Section 7.5.4 of IEC 60904-8 at about 950 nm (15%-curve) and 1000 nm (5%-curve), respectively. The deviation increases until reaching a fixed plateau at about 1070 nm. From this wavelength on, the excess charge carrier distribution is uniform throughout the bulk and thus the injection properties do not change any more for longer wavelengths. In contrast with the simulation, the measured data show a further increase for wavelengths above 1150 nm. We attribute this to an increased measurement uncertainty due to the strongly decreasing absolute signal of the differential spectral responsivity.

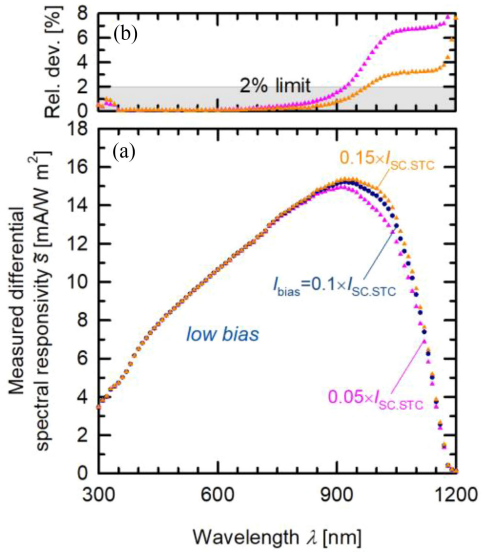

Fig. 9. Measured data: (a) Spectral responsivity curves according to the low bias approach: 5%-, 10%- and 15%-curves. (b) Relative deviation of the 0.10- and 0.15-$I_{\mathrm{sc.STC}}$ curves to the 0.10-curve, exceeding the 2% limit at wavelengths larger than 950 nm (15%-curve) and 1000 nm (5%-curve).

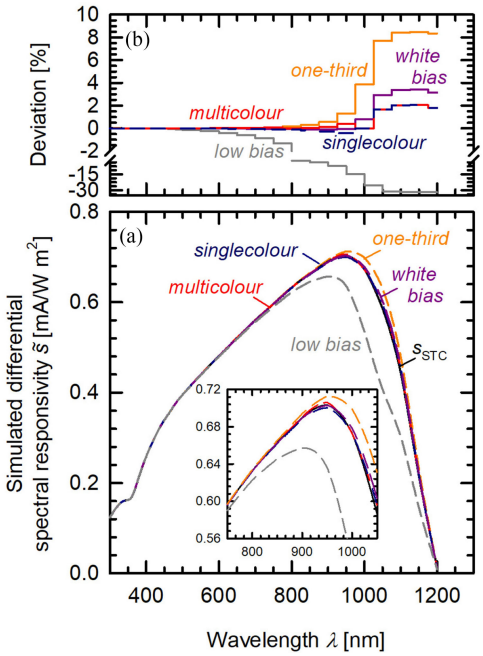

Fig. 10. (a) Simulated differential spectral responsivity curves at bias irradiances corresponding to the simplifications as defined in the IEC 60904-8 standard, for comparison the $s_{\mathrm{STC}}(\lambda)$ curve is shown as a black line, (b) corresponding deviations of $\tilde{s}(\lambda, I_0)$ from $s_{\mathrm{STC}}(\lambda)$ for all simplifications.

C. Deviation of Simplifications to Complete Differential Spectral Responsivity Procedure

At the bias currents determined above for the different simplifications, we simulate and measure the corresponding differential spectral responsivity curves. The results are shown in Fig. 10(a) (simulation) and Fig. 11(a) (measurement), respectively. For comparison, we also show the absolute spectral responsivity s_{STC} determined by the complete procedure.

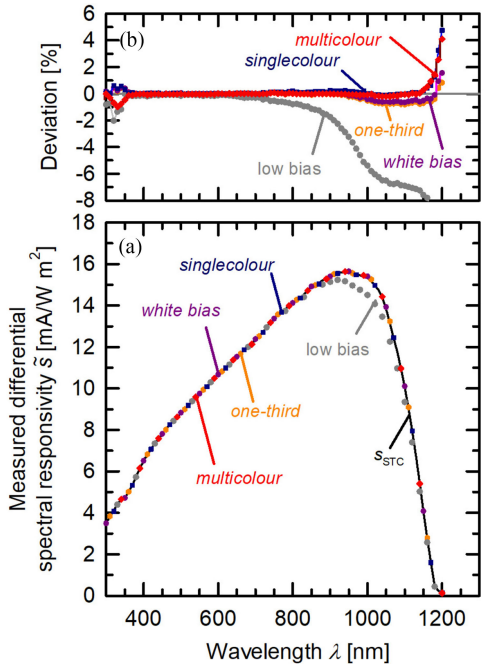

Fig. 11. (a) Measured differential spectral responsivity curves at bias irradiances corresponding to the simplifications as defined in the IEC 60904-8 standard, for comparison the $s_{\mathrm{STC}}(\lambda)$ curve is shown as a black line, (b) corresponding deviations of $\tilde{s}(\lambda, I_0)$ from $s_{\mathrm{STC}}(\lambda)$ for all simplifications.

For both the simulated and the measured datasets, the spectral responsivity curves related to the multicolor, the singlecolor, and the white bias approach are in very good agreement with the $s_{\mathrm{STC}}(\lambda)$ curve. For the measured data, also the one-third approach shows a good agreement. This is different for the simulative approach; here, the one-third approach shows a larger deviation with an overestimation in the spectral responsivity for wavelength above 900 nm. However, this is consistent with the considerably higher bias current as determined for this simplification in the simulative approach.

To quantify the deviations of the simplifications from complete approach, Fig. 10(b) (simulation) and 11(b) (measurement) show the relative deviation of differential spectral responsivity curves related to the simplifications relative to the $s_{\mathrm{STC}}(\lambda)$ curve. Note, for the interpretation of the measured data, we focus on the 400–1150 nm range due to the increased uncertainty of wavelengths outside this interval.

The smallest deviations are obtained by the multi- and singlecolor approaches (red and blue lines) showing a maximum deviation of 2.1% (simulation) and 0.3% (measurement), respectively. For simulation and measurement, the second smallest maximum deviation is obtained by the white bias approach (purple lines), which leads to maximum deviations of about 3.4% for the simulation and 0.6% for the measurement, respectively. The one-third (orange line) approach shows a much larger maximum deviation of up to 8.5% for the simulated data. In contrast, the one-third approach only reaches a deviation of 0.8% for the measured cell.

The largest deviation arises from the low bias approach (gray line) with a maximum deviation of 32% for the simulative approach and more than 7% for the measurement. In this case,

TABLE I
IMPACT OF SIMPLIFICATIONS ON THE SHORT-CIRCUIT CURRENT RELATIVE TO $I_{\mathrm{SC.STC}}$ AND ON THE SPECTRAL MISMATCH FACTOR MM

Approach	I_0 [mA]	MM (Xe + Ha)	MM (filtered-Xe)	$I_{\mathrm{SC}}/I_{\mathbf{SC.STC}}$
Simulation				
Complete	1.9, 3.8, 7.3, 13.5, 15.8, 24.0, 32.3, 48.9	1.00294	0.98855	1.0000
Multicolor	12.4, 11.9, 11.1	1.00298	0.98791	1.0018
Singlecolor	11.4	1.00299	0.98760	1.0006
White bias	11.7	1.00296	0.98724	1.0026
One-third	13.5	1.00289	0.98595	1.0099
Low bias	2.03, 4.06, 6.09	1.00357	0.99686	0.9516
Measurement				
Complete	78, 189, 825, 1873, 3050, 9024, 9971	1.00101	0.98875	1.0000
Multicolor	3282, 3162, 2851	1.00093	0.98890	1.0004
Singlecolor	2861	1.00105	0.98873	0.9993
White bias	3142	1.00102	0.98859	1.0005
One-third	3050	1.00103	0.98863	1.0001
Low bias	458, 915, 1373	1.00130	0.99007	0.9862

the deviations do not solely affect the long wavelength regime but already start at wavelengths of around 600 nm for both, simulation and measurement.

VII. IMPACT ON SPECTRAL MISMATCH CORRECTION

While in primary solar cell calibration based on the complete spectral responsivity procedure, the spectral responsivity is used to provide the short-circuit current of the solar cell under test, in secondary solar cell calibration the spectral responsivity is predominantly used to calculate the spectral mismatch factor. Consequently, it is of general interest to quantify the impact of the deviations in the spectral responsivity curves on the spectral mismatch factor for the different simplifications.

For the calculation of the spectral mismatch factor, we consider the case that the solar simulator is calibrated with a typical WPVS reference solar cell. For the solar simulator spectrum, we assume a class A xenon–halogen (Xe + Ha) two-lamp system as well as a class A filtered xenon (filtered-Xe) flash system. The resulting MMs are given in Table I.

Using the simulated $s_{\mathrm{STC}}(\lambda)$ data as determined from the complete differential spectral responsivity procedure, we obtain an MM of 1.00294 for the Xe + Ha spectrum and 0.98855 for the filtered-Xe spectrum as a reference. For the Xe + Ha spectrum, the deviation to this reference values are below 0.005% for the multicolor, the singlecolor, the white bias, and the one-third approach. Only the low bias approach yields a larger deviation of 0.063%. However, even this is a considerably small value, which is still suitable for an MM correction in secondary solar cell calibration. Using the filtered-Xe spectrum for the MM calculation, we obtain considerably larger MMs as expected for a less ideal spectrum. In addition, also the deviations relative to the reference value are increased by up to one order of magnitude: 0.064% (multicolor approach), 0.095% (singlecolor approach), 0.13% (white bias approach), 0.26% (one-third approach), and 0.83% (low bias approach).

For the measured data, the use of $s_{\mathrm{STC}}(\lambda)$ as determined from the complete procedure yields MMs of 1.00101 for the Xe + Ha and 0.98875 for the filtered-Xe spectrum, respectively. Compared with the simulated data, the deviation of the MMs corresponding to different simplifying approaches is smaller.

In addition, Table I also shows $I_{\mathrm{SC}}/I_{\mathrm{SC.STC}}$ ratios as obtained by integrating the product of the tabulated AM1.5G spectrum and the $s_{\mathrm{STC}}(\lambda)$ curve as well as the differential spectral responsivity curves $\tilde{s}(\lambda, I_0)$ related to the different simplifications. As expected, the deviations are much larger than the deviations of the spectral mismatch factor only. The largest deviation with 4.8% (simulation) and 1.4% (measurement) is again obtained for the low bias approach. The other approaches show deviations from 0.06% to 0.99% for the simulations as well as deviations of only 0.04% to 0.07% for the measured data. Note that in today's primary solar cell calibration, using short-circuit currents directly calculated from the spectral responsivity data uncertainties in the range of 0.5% to 0.8% ($k = 2$) are reported. In order to reach such low values, a deviation due to the use of a simplification should be below 0.1%.

It is of no surprise that the multicolor approach yields the best results since the bias irradiance setpoint is adjusted over the spectral range to best meet the requirement of each wavelength interval. The singlecolor approach yields equally well results, because it uses a bias ramp wavelength close to maximum of the spectral responsivity curve. This ensures that the wavelength region with highest weight in the spectral mismatch calculation uses the appropriate bias irradiance.

In contrast, the white bias approach utilizes a broadband spectrum and thus probes for nonlinearity over the whole wavelength range with a weighting of the wavelengths corresponding to all wavelengths in the white light spectrum. One consequence is that the weighting of those parts of the $\tilde{s}(\lambda)$ curve that deviate from $s_{\mathrm{STC}}(\lambda)$ are "suppressed" by those regions showing a good agreement. As a result, the setpoint bias current $I_{\mathrm{bias}}(E_0)$ comes out higher corresponding to a singlecolor bias current that one would determine from a bias ramp at 900 nm. Note that this is a wavelength slightly below the maximum of the spectral responsivity curve.

VIII. CONCLUSION

We compared the simplifications for determining spectral responsivity curves defined in the IEC 60904-8 standard with the complete differential spectral responsivity procedure by means of simulation and experiment. For both, simulation and experiment, we studied solar cells with a strong but still realistic nonlinearity. In both cases, an injection-dependent rear surface recombination velocity caused the nonlinearity.

For a front junction device, as investigated in this paper, the lowest deviation to the spectral responsivity curve of the complete procedure was obtained from the multicolor and the singlecolor approach determining $I_{\mathrm{bias}}(E_0)$ from bias ramps measured at different wavelengths (multicolor) or one wavelength close to the maximum spectral responsivity (singlecolor). The

second best result was determined for the white bias approach. The one-third approach already showed much larger deviations in the simulated data but was similar to the white bias approach for the measured solar cell. Only the low bias approach showed considerably larger deviations of more than 32% for the simulated and 7% for the measured data. In order to justify the use of the low bias approach, it is strongly recommended to test for linearity by fulfilment of the 2%-limit as defined in the IEC 60904-8 standard.

Practical laboratory experience [22] shows that the bias irradiance at which the differential spectral responsivity equals the spectral responsivity often comes out to be about 300 W/m^2. This practical experience has been confirmed by our work showing the general suitability of the one-third approach as a reliable simplification.

In contrast, the low bias approach comes out to be not suitable for the precise determination of the spectral responsivity of nonlinear solar cells. However, as the IEC 60904-8 standard introduces the 2%-limit, the approach can be used to measure linear solar cells.

The most relevant conclusion we can draw from this study is that the simplifications of the complete differential spectral responsivity procedure proposed in the IEC 60904-8 standard can be used in secondary solar cell calibration. The application order proposed in the standard coincides with increasing maximum deviations found in this paper: multicolor approach, singlecolor approach, white bias approach, one-third approach, and low bias approach.

Based on our experience, we are confident that nonlinear solar cells with a stronger bias-dependent spectral responsivity as investigated here are rare. Consequently, for the majority of solar cell calibrations, the determined spectral responsivity deviations of the different simplifications to the complete procedure can be regarded as upper limits.

ACKNOWLEDGMENT

The authors would like to acknowledge the continuous support of R. Brendel for the ISFH Calibration and Test Center (CalTeC). This work was part of the European Metrology Research Programme (EMRP). The EMRP is jointly founded by the EMRP participating countries within EURAMET and the European Union.

REFERENCES

[1] *Photovoltaic Devices-Part 8: Measurement of Spectral Responsivity of a Photovoltaic (PV) Device*, IEC 60904-8:2014, Ed. 3.0, 2014.

[2] "Standard procedures for terrestrial photovoltaic performance measurements," Specification No. 101, Issue 2, Commission Eur. Community, Brussels, Belgium, 1980.

[3] *Photovoltaic Devices-Part 3: Measurement Principles for Terrestrial Photovoltaic (PV) Solar Devices With Reference Spectral Irradiance Data*, IEC 60904-3:2016, Ed. 3.0, 2016.

[4] J. Metzdorf, S. Winter, and T. Wittchen, "Radiometry in photovoltaics: Calibration of reference solar cells and evaluation of reference values," *Metrologia*, vol. 37, pp. 573–578, 2000.

[5] J. Hohl-Ebinger, G. Siefer, and W. Warta, "Non-linearity of solar cells in spectral response measurements," in *Proc. 22nd Eur. Photovolt. Sol. Energy Conf.*, Milan, Italy, 2007, pp. 422–424.

[6] A.G. Aberle, S. Glunz, and W. Warta, "Impact of illumination level and oxide parameters on Shockley-Read-Hall recombination at the Si-Si0_2 interface," *J. Appl. Phys.*, vol. 71, no. 9, pp. 4422–4431, 1992.

[7] *Photovoltaic Devices-Part 7: Computation of the Spectral Mismatch Correction for Measurements of Photovoltaic Devices*, IEC 60904-7:2008 Ed. 3.0, 2008.

[8] *Sentaurus, User Manual*, Synopsys Inc., Mountain View, CA, USA, 2016.

[9] P. P. Altermatt, "Models for numerical device simulations of crystalline silicon solar cells—A review," *J. Comput. Electron.*, vol. 10, pp. 314–330, 2011.

[10] A. Richter, S.W. Glunz, F. Werner, J. Schmidt, and A. Cuevas, "Improved quantitative description of Auger recombination in crystalline silicon," *Phys. Rev. B*, vol. 86, no. 16, 2012, Art. no. 165202.

[11] M. Rüdiger, M. Rauer, C. Schmiga, and M. Hermle, "Effect of incomplete ionization for the description of highly aluminum-doped silicon," *J. Appl. Phys.*, vol. 110, no. 2, 2011, Art. no. 024508.

[12] P. Rosenits, T. Roth, and S.W. Glunz, "Erratum on Determining the defect parameters of the deep aluminum-related defect center in silicon [Appl. Phys. Lett. 91, 122109 (2007)]," *App. Phys. Lett.*, vol. 99, no. 23, 2011, Art. no. 239904.

[13] Y. Chen, H. Shen, and P.P. Altermatt, "Analysis of recombination losses in screen-printed aluminum-alloyed back surface fields of silicon solar cells by numerical device simulation," *Sol. Energy Mater. Sol. Cells*, vol. 120, pt. A, pp. 356–362, 2014.

[14] H. Steinkemper *et al.*, "Adapted parameterization of incomplete ionization in aluminum-doped silicon and impact on numerical device simulation," *J. Appl. Phys.* vol. 117, no. 7, 2015, Art. no. 074504.

[15] K. Bothe, R. Sinton, and J. Schmidt, "Fundamental boron–oxygen-related carrier lifetime limit in mono-and multicrystalline silicon," *Prog. Photovolt., Res. Appl.*, vol. 13, no. 4, pp. 287–296, 2005.

[16] A. Piechulla *et al.*, "Low pressure diffusions for high quality emitter formation in advanced p-and n-type solar cells," in *Proc. 31st Eur. Photovolt. Sol. Energy Conf.*, Hamburg, Germany, 2015, pp. 420–424.

[17] R. Bock, P.P. Altermatt, J. Schmidt, and R. Brendel, "Formation of aluminum–oxygen complexes in highly aluminum-doped silicon," *Semicond. Sci. Technol.*, vol. 25, 2010, Art. no. 105007.

[18] B. T. Phong, "Illumination for computer generated pictures," *Commun. ACM*, vol. 18, no. 6, pp. 311–317, 1975.

[19] L. E. Black and K. R. McIntosh, "Modeling recombination at the Si–Al_2-O_3 interface," *IEEE J. Photovolt.*, vol. 3, no. 3, pp. 936–943, Jul. 2013.

[20] C. Osterwald *et al.*, "The world photovoltaic scale: An international reference cell calibration program," *Prog. Photovolt., Res. Appl.*, vol. 7, no. 4, pp. 287–297, 1999.

[21] T. Dullweber *et al.*, "Towards 20% efficient large-area screen-printed rear-passivated silicon solar cells," *Prog. Photovolt., Res. Appl.*, vol. 20, no. 6, pp. 630–637, 2012.

[22] B. Fischer, "Loss analysis of crystalline silicon solar cells using photoconductance and quantum efficiency measurements," Ph.D. dissertation, Dept. Phys., Univ. Konstanz, Konstanz, Germany, 2003.

Karsten Bothe studied physics with the TU Braunschweig, Braunschweig, Germany; the University of Sussex, Brighton, U.K.; and the University of Oldenburg, Oldenburg, Germany. He received the Diploma degree in physics from the University of Oldenburg, in 2001, and the Ph.D. degree in oxygen-related trapping and recombination centres in boron-doped crystalline silicon from the University of Hannover, Hannover, Germany, in 2006.

He joined the Institute for Solar Energy Research Hamelin (ISFH), Emmerthal, Germany, in 2001. After being with the Nara Institute of Science and Technology, Nara, Japan, as a Research Fellow, in 2007, he became the head of the solar cell characterization group, ISFH. After supervising pioneering work on camera-based luminescence imaging techniques for the characterization of silicon wafers and solar cell, he worked on the development of combined algorithms and measurement techniques for a quantitative local loss analysis of crystalline silicon solar cells. Since 2016, he has been the head of the solar cell calibration laboratory with the ISFH Calibration and Test Center (CalTeC). He has authored and coauthored more than 150 scientific papers in leading journals and conferences. His current research interest is calibrated measurement of the characteristic parameters of crystalline silicon solar cells.

David Hinken studied physics at the University of Hannover, Hannover, Germany, and the University of La Laguna, San Cristóbal de La Laguna, Spain. He received the Diploma degree in physics from the University of Hanover in 2007, and the Ph.D. degree in physics from the University of Hanover with a thesis about luminescence-based characterization of crystalline silicon solar cells in 2012.

In the Solar Cell Characterization Group of the Institute for Solar Energy Research Hamelin (ISFH), Emmerthal, Germany, he worked on algorithms for a quantitative loss analysis of solar cells by means of solar cell modeling with experimentally determined input parameters. In 2015, he joined the solar cell calibration laboratory of the ISFH Calibration and Test Center (CalTeC) and is responsible for the solar cell calibration equipment. His current research interest is precise measurement of the characteristic solar cell parameters, including the determination of the accompanied measurement uncertainty.

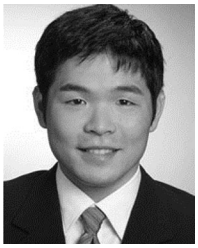

Byungsul Min received the Diploma degree in electrical engineering from the RWTH Aachen University, Aachen, Germany, in 2009, and the Ph.D. degree in electrical engineering from the RWTH Aachen University in 2014, with a thesis on modeling of carrier recombination in heavily phosphorus-doped emitters of industrial silicon solar cells.

Afterward, he joined the Institute for Solar Energy Research Hamelin, Emmerthal, Germany, carrying out research and development work on industrial PERC solar cells. His current research interests include fabrication and characterization of industrial silicon solar cells and high-efficiency solar cells, in particular with passivating contacts.

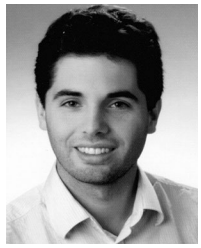

Carsten Schinke received the Diploma degree from the University of Hannover, Hannover, Germany, in 2010, and the Ph.D. degree from the University of Hannover, Hannover, Germany, in 2015, both in physics.

Afterward, he worked with the Institute for Solar Energy Research Hamelin (ISFH), Emmerthal, Germany, on the determination of the measurement uncertainty of the absorption coefficient of crystalline silicon. Since 2015, he has been the head of the solar cell simulations team with the Institute for Solid State Physics at the University of Hannover (ISFH), Emmerthal, Germany, and has also been working with the solar cell calibration laboratory at the ISFH Calibration and Test Center (CalTeC). His current research focuses on optical modeling of solar cells and modules.